Desalination and Water Treatment
www.deswater.com

doi: 10.5004/dwt.2023.30138

315 (2023) 314–326
December

Preparation and characterization of activated carbon from *Balanites aegyptiaca* seed shell for the removal of 2,4-dichlorophenoxyacetic acid herbicide from aqueous solution

Omer El-Amin Ahmed Adam[a,*], Abdullah Sarhan Al-Shammari[b]

[a]*Department of Chemistry, Faculty of Science and Arts in Baljurashi, Al-Baha University, P.O. Box: 1988, Al-Baha, Saudi Arabia, Tel.: +966558167205; email: omaramin1967@gmail.com*
[b]*Department of Physics, College of Science, University of Hail, P.O. Box: 2440, Hail, Saudi Arabia, email: ashammari@uoh.edu.sa*

Received 5 July 2023; Accepted 8 November 2023

ABSTRACT

This research investigates the potential of *Balanites aegyptiaca* (desert date) seed shells, an abundant renewable bio-waste product, as a precursor for producing low-cost activated carbon for the removal of the herbicide 2,4-dichlorophenoxyacetic acid (2,4-D) from aqueous solution via batch technique adsorption. The chemical activation process was carried out using $ZnCl_2$ as an activating agent at 700°C and 1:2 impregnation ratio. The activated carbon was characterized by "Boehm" titration, measurements of pH of the point zero charge, scanning electron microscopy, Fourier-transform infrared spectroscopy and specific surface areas (S_{MB}) by methylene blue adsorption. The effects of initial herbicide concentration, contact time, solution pH, and solution temperature on the sorption capacity were investigated. Equilibrium data were fitted to the Langmuir, Freundlich, Temkin, Redlich–Peterson, Sips, and Toth models. The highest correlation coefficient (R^2) values were obtained from Temkin model, with values of 0.997, 0.999, and 0.996 at 298.15, 308.15, and 318.15 K, respectively. The enthalpy change ($\Delta H°$), entropy change ($\Delta S°$) and free energy change ($\Delta G°$) were also evaluated. The negative value of $\Delta G°$ shows that the adsorption process is spontaneous, and the positive value of $\Delta H°$ shows the endothermic nature of the process. The experimental data were tested through the pseudo-first-order, pseudo-second-order, and intraparticle diffusion models. The pseudo-second-order kinetic model was the most fitting to the kinetics data ($R^2 > 0.981$). Results showed that *Balanites aegyptiaca* seed shell activated carbon is very efficient for the removal of 2,4-D from aqueous solutions.

Keywords: *Balanites aegyptiaca*; Activated carbon; Adsorption isotherms; 2,4-Dichlorophenoxyacetic acid

1. Introduction

The presence of halogenated organic contaminations in water poses a significant danger to aquatic life [1]. Nanofiltration, photocatalytic degradation, electrocoagulation, photo-Fenton, biological processes, ultrasound, sedimentation, and adsorption are commonly used methods for treating contaminated water holding pesticides [2,3].

The most used adsorbent is activated carbon, in its powdered or granular form. Its particles have a porous structure consisting of interconnected macropores, mesopores, and micropores. The high surface area of these structures allows for a greater number of active sites, which can effectively adsorb a wide range of organic molecules. This makes activated carbons highly versatile and capable of addressing

* Corresponding author.
Permanent Address: Chemistry Department, University of Kassala, P.O. Box: 266, Kassala, Sudan

various environmental and industrial challenges [4]. Due to its high removal efficiency, activated carbon has become extensively used for reclaiming pollutant-laden wastewater in the past few decades.

One reason why activated carbon has not been extensively used in large-scale industrial applications is the cost associated with their production. The manufacturing process involves heating carbonaceous materials, such as coal or coconut shells, at high temperatures to create a porous structure. This process requires significant energy input and specialized equipment, making it relatively expensive compared to other adsorbents [5].

Nowadays, the necessity to find sustainable adsorbents with zero damage to the environment is the economic and environmental challenge faced by researchers. Various types of waste materials are used to produce highly effective activated carbons. To highlight recent achievements related to the topic, we can present some exemplary research reports. Peanut shells (PNS), coffee husks (CH), corn cobs (CC), and banana peels (BP) were converted into multi-substrate activated carbon to efficiently remove CO_2 [6]. Other researchers obtained the activated carbons from rice straw [7], hazelnut husks [8], hazelnut shell [9], Plantain (*Musa paradisiaca*) [10], and cassava sieve biomass [11] for the removal of different pollutants from an aqueous solution. Another noteworthy research report by Wu et al. [12] explored the use of agricultural waste, specifically rice straw, as a precursor for activated carbon synthesis. Lately, activated carbons made from *Balanites aegyptiaca* seed shells are appearing in the literature. They have been used for the removal of crystal violet [13], hexavalent chromium [14], and Hg^{2+} and As^{3+} [15].

The herbicide 2,4-dichlorophenoxyacetic acid (2,4-D) is popularly used for generic weed control owing to its low cost and high selectivity [16]. It is used for post-emergent control of broad-leaf weeds in both agricultural and household applications. 2,4-D may endanger human and animal health through exposure to polluted water, air, soil, and food [17]. It is the active ingredient in several herbicide formulations recommended for broadleaf weeds control.

The maximum allowed concentration of 2,4-D in aqueous medium is 0.03 mg/L [18]. The main properties of 2,4-D include relative toxicity with high movability, durability, non-volatility, and high solubility in aqueous medium [19].

This study investigates the isotherms, kinetics, and thermodynamics of 2,4-D herbicide adsorption onto *Balanites aegyptiaca* seed shells activated carbon to further understand its efficacy as a remediation technology.

2. Experimental set-up

2.1. Chemicals and reagents

2,4-Dichlorophenoxyacetic acid of 98% purity was used as an adsorbate. Zinc chloride of 98% purity is used as a chemical activating agent. Hydrochloric acid (HCl, 37%) and sodium hydroxide (NaOH, 98%–100%) were used for pH adjustment. Methylene blue (λ_{max}: 665 nm) of 99.8% purity was used for surface area determination. All chemicals were purchased from Sigma-Aldrich. Double distilled water was used to prepare the solutions.

2.2. Adsorbent

Balanites aegyptiaca seeds were obtained from local market in Gezira Province (Central Sudan). The samples were soaked in water for 5 h, washed thoroughly to remove the pulp, dried, weighed, grinded and sieved into particles sizes ranging between 1.00–2.00 mm. The sample was then heated at 220°C for 2 h and the produced char was ground into fine powder by a kitchen mixer. The char was impregnated with $ZnCl_2$ (Char: $ZnCl_2$ = 1:2, wt./wt.). The impregnation was followed by carbonization at 700°C for 2 h in a crucible under N_2 environment. The resulting material (activated carbon) was soaked overnight in a 0.1 M HCl solution to extract any residual $ZnCl_2$ from inner pores, and then washed with worm distilled water until a pH of 6.5–7.0 is reached. The product sample *Balanites aegyptiaca* seed shell activated carbon (BAC) was dried at 105°C for 24 h. Finally, the sample was grinded and sieved to a particle size less than 0.212 mm and then preserved in desiccator before characterization and application.

2.3. Characterization of BAC

2.3.1. Determination of oxygen containing functional groups

The quantification of surface functional groups on BAC was conducted by following a standardization procedure using Boehm titration method [20]. An adsorbent mass of 0.2 g (m) was mixed with 25 mL of NaOH (0.10 M), Na_2CO_3 (0.10 M), $NaHCO_3$ (0.05 M), and HCl (0.10 M) in a series of 100-mL Erlenmeyer flasks. The flasks were sealed and shaken for 48 h in a LabTech Shaking Incubator (LSI-1005R) at 250 rpm. After filtering the mixtures, 10 mL of each filtrate was pipetted and the excess of base or acid was titrated by 0.10 M solution of HCl or NaOH, respectively.

2.3.2. Point of zero charge

The point of zero charge (pH_{pzc}) was studied by pH drift method using a glass electrode pH meter (Jenway 3510, Cole-Parmer, Essex, UK) calibrated by buffers of pH 4, 7 and 10 [21]. By preparing aliquots with 50 mL of 0.01 M KNO_3 solution in various flasks and adjusting their pH from 2 to 12 using either HCl or NaOH, we were able to create a range of acidic and alkaline conditions. Once the desired pH value was achieved and stabilized, we introduced 0.15 g of the carbon sample into each flask. The flasks were then sealed and placed in a shaker for three days, allowing sufficient time for any chemical reactions or interactions between the carbon sample and the surrounding solution to occur.

To ensure accurate results, blank tests were also conducted without adding any carbon samples. These blank tests helped us determine if any changes in pH were solely due to the presence of CO_2, which could potentially influence the final pH readings. After three days of shaking, the final pH of each solution was determined. The pH_{pzc} value is the point where the curve pH_{final} vs. ΔpH crosses the horizontal line of $pH_{initial}$.

2.3.3. Surface area determination

The specific surface area of BAC was found by the method of methylene blue (MB) adsorption [22,23].

To perform these experiments, a series of 50 mL bottles were used. Each bottle was filled with 50 mL of methylene blue solution with concentrations ranging from 5.0 to 50.0 mg/L. In total, there were 10 different standard concentrations used. In addition to the MB solution, each bottle contained 0.01 g of BAC. This amount was carefully measured and added to ensure consistent conditions for all experiments.

To ensure proper mixing and contact between the solution and BAC, the stoppered bottles were placed in a LabTech Shaking Incubator (LSI-1005R, DAIHAN Labtech Co., Ltd., Namyangju, Korea) set at a temperature of 25°C. The incubation period lasted for 24 h, allowing sufficient time for adsorption to occur. After which a 3.0 mL portion of each solution was withdrawn and filtered. The MB concentrations were determined spectrophotometrically using UV-Visible Spectrophotometer (APEL PD-303UV, APEL Co., Ltd., Saitama, Japan).

2.3.4. Fourier-transform infrared spectroscopy analysis

Fourier-transform infrared spectroscopy (FTIR) spectroscopy was employed to pinpoint the functional groups on BAC surface. The spectra were recorded in the range of 400–4,000 cm^{-1}, which is a typical range for FTIR analysis. To carry out the measurements, a FTIR spectrophotometer (Thermo Scientific™ Nicolet™ iS™50, Madison, USA) was utilized. The spectra were recorded in the range between 4,000 and 400 cm^{-1} as KBr pellets.

2.3.5. Scanning electron microscopy analysis

The surface morphology of BAC was figured out using JEOL scanning electron microscopy (SEM) equipment (JEOL, JSM-6490, Tokyo, Japan).

2.4. Adsorption experiments

Batch adsorption experiments were conducted by mixing a fixed amount of BAC activated carbon with 25 mL of 2,4-D solutions of the desired concentration in 50 mL glass flasks. During the period of equilibration, the flasks were stoppered and kept in a thermostatic shaking incubator. The amount of adsorption at equilibrium (q_e mg/g) was calculated according to the expressions:

$$q_e = \frac{\left(C_0 - C_e\right)}{m} \cdot V \tag{1}$$

where C_0 and C_e are the initial and equilibrium concentrations (mg/L), V the volume of solution (L), m is the mass of the carbon material (g). Both the initial and final equilibrium concentrations of 2,4-D were determined using a single-beam UV/Visible spectrophotometer with a 1.0 cm light-path quartz cell.

2.5. Effect of Initial pH on 2,4-D adsorption

To investigate the influence of pH on the adsorption of 2,4-D by BAC in the aqueous phase, different pH values ranging from 2 to 12 (in intervals of 2) were used. The herbicide concentration was set at 100 mg/L, the adsorbent dose was 0.15 g per 50 mL solution, and the contact time was 3 h in a shaking incubator at 25°C. The pH was adjusted by adding a few drops of diluted 0.1 N NaOH or 0.1 N HCl and measured using Jenway 3510 pH meter.

3. Results and discussion

3.1. Characterization of BAC

Table 1 summarizes quantitative information on the acidic and basic groups on the adsorbent surfaces; the information was obtained through Boehm titration. Generally, acidic and basic groups coexist on the surface of any adsorbent. The BAC used in this study is considered acidic because the total number of acidic groups is more than the basic sites.

To find the pH_{pzc}, the pH drift method was used. The experimental results are shown in Fig. 1. The pH_{pzc} is the point where the curve of ΔpH vs. $pH_{initial}$ intersects the horizontal axes of $pH_{initial}$. The pH_{pzc} value for BAC was found to be 6.8, which coincided with the results of Boehm's titration.

The specific surface area of BAC was calculated from the Langmuir adsorption isotherm (Fig. 2) by Eq. (2):

$$S_{MB} = \frac{\left(q_m \times a_{MB} \times N_A \times 10^{-20}\right)}{M} \tag{2}$$

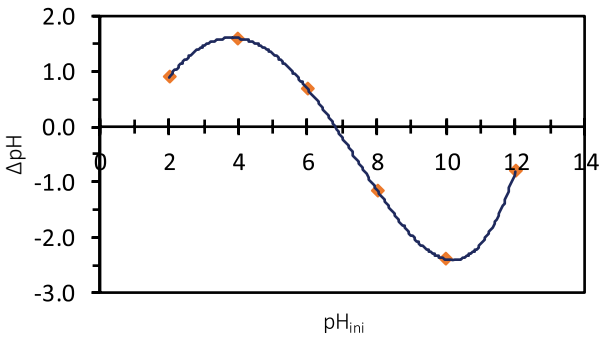

Fig. 1. Point of zero charge of BAC, determined using the pH drift method.

Table 1
Boehm titration results and surface density of functional groups and pH_{pzc} of BAC

Basic groups (μmol/g)	Lactonic groups (μmol/g)	Carboxylic groups (μmol/g)	Phenolic groups (μmol/g)	Total acidic groups (μmol/g)	Total functional groups (μmol/g)	Density of group on the surface (group/nm^2)	pH_{pzc}
850.0	150.0	200.0	650.0	1,000.0	1,850.0	2.67	6.8

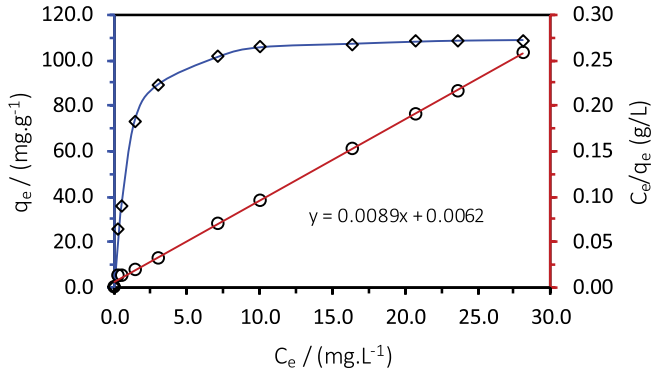

Fig. 2. Adsorption isotherm (blue) and Langmuir isotherm (red) for methylene blue onto BAC at 298.15 K.

where S_{MB} is the specific surface area in m^2/g; q_m is the amount of methylene blue monolayer adsorbed at the surface of adsorbent in mol/g calculated from Langmuir isotherm (Fig. 2). a_{MB} is the surface area occupied by one molecule of methylene blue = 197.2 Å^2 [24], N_A is Avogadro's number, 6.02×10^{23} mol^{-1}, and M is the molecular weight of methylene blue. The surface area of BAC was found to be 417.0 m^2/g.

The use of FTIR spectroscopy was crucial for identifying and characterizing the functional groups present on the surface of BAC. By analyzing the infrared spectra obtained, valuable information about the chemical composition and structure of BAC could be deduced.

Fig. 3a shows the FTIR spectrum of 2,4-D. Absorption band seen at 1,732.20 cm^{-1} corresponds to the vibration of the (C=O) of the carboxylic group. The aromatic C=C bond is marked by a noticeable peak at 1,476.31 cm^{-1}, while the presence of a band at 1,229.91 cm^{-1} can be attributed to the concurrent O–H deformation and C–O stretching vibration. The presence of the antisymmetric and symmetric vibrations of C–O–C results in two bands located at 1,310.36 and 1,092.00 cm^{-1}, respectively [25]. The peak at 695.00 cm^{-1} is a sign of C–Cl stretching [26].

Fig. 3b shows the FTIR spectrum of raw BAC. The 1,648 cm^{-1} band seen in the aromatic region may indicate either C=C or C=N vibrations, while the absorption peaks at 1,597 and 1650 cm^{-1} are linked to C=O stretching [27]. Peaks observed at frequencies of 1,519 and 1,338 cm^{-1} can possibly be explained by the C=C stretching of the aromatic skeletal modes [28]. The bending modes of O–C–H, C–C–H and C–O–H can be acknowledged as the cause of the peak at 1,228 cm^{-1} [29]. The 1,047–988 cm^{-1} region features peaks resulting from C–O stretching vibrations [30].

The vibration modes at 1,111 and 1,047 cm^{-1} point towards C–O stretching for alcohols/phenols molecules [31,32]. These results agree with those obtained through Boehm titrations.

Post adsorption, there was a rise in frequency from 1,519 to 1,520 cm^{-1}, 1,338 to 1,339 cm^{-1}, and 8,31 to 832 cm^{-1}, while peaks at 1,228, 589, and 529 cm^{-1} slightly shifted to lower frequency bands of 1,226, 586 and 528 cm^{-1}, respectively. It can be seen from the FTIR spectra of BAC before and after adsorption (Fig. 3b and c) that a considerable number of functional groups have shifted positions to other bands which shows the possible interaction of those active functional groups with that of 2,4-D molecules.

The SEM technique played a crucial role in unraveling the morphology of BAC sample both pre- and post-adsorption process (Fig. 4a and b). SEM is a powerful imaging technique that provides high-resolution, three-dimensional images of samples. It works by bombarding the sample with a focused beam of electrons and collecting the signals emitted from the surface. This enables scientists to visualize the topography, size, shape, and even elemental composition of the sample. Numerous pores were discovered on the samples surface due to the release of most organic volatiles during analysis, leaving behind a ruptured carbon surface.

3.2. Effect of contact time

In all transfer phenomena, the essential parameter to consider is the contact time. The adsorption capacity of 2,4-D onto BAC at concentration 80 mg/L and at three different temperatures is shown in Fig. 5. Initially, as the contact time increases, the adsorption capacity of 2,4-D onto BAC also increases rapidly. This can be attributed to the availability of more time for the adsorbate molecules to encounter the adsorbent surface. However, as the contact time continues to increase, it is observed that the rate of increase in adsorption capacity slows down. This could be due to several factors. One possibility is that most of the easily accessible active sites on BAC have already been occupied by 2,4-D molecules during the initial rapid phase.

3.3. Equilibrium modeling

Adsorption isotherms are mathematical models that describe the relationship between the adsorbate concentration in solution and the amount adsorbed onto the adsorbent material at equilibrium. Six different adsorption isotherm models were considered in this study: Langmuir, Freundlich, Temkin, Redlich–Peterson, Sips, and Toth, since they are the most studied and they are the best understood models. Each model offers unique insights into the adsorption process and provides valuable information about the interaction between the adsorbate and adsorbent.

3.3.1. Two-parameter models

3.3.1.1. Langmuir isotherm

The Langmuir isotherm model assumes a monolayer adsorption on a homogeneous surface, where the adsorption sites are energetically equivalent. It describes the formation of a saturated layer of adsorbate molecules on the surface, with no further adsorption occurring once this layer is formed [33]. The linear form of Langmuir isotherm equation is given as:

$$\frac{C_e}{q_e} = \frac{1}{q_m K_L} + \frac{1}{q_m} C_e \tag{3}$$

where q_m is the maximum adsorption capacity (mg/g), and K_L is the equilibrium adsorption constant related to the free energy of the adsorption (L/mg). The value of q_m, K_L constants

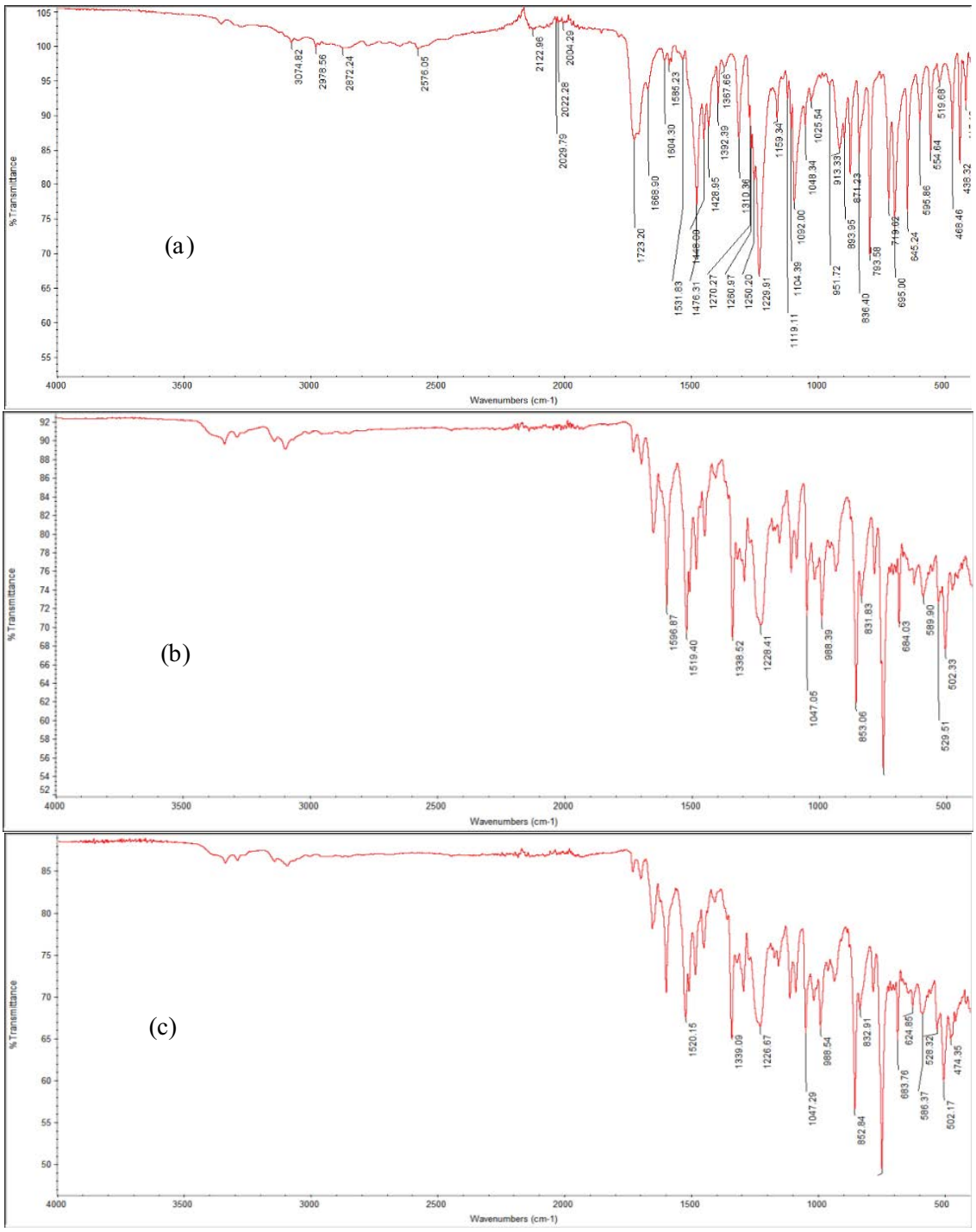

Fig. 3. Fourier-transform infrared spectrum of (a) 2,4-D, BAC before (b) and after (c) 2,4-D adsorption.

and R^2 are presented in Table 2. The essential feature of the Langmuir isotherm can be expressed with a dimensionless constant (R_L) that is referred to as separation factor or equilibrium parameter. It is defined by Xiao et al. [34] Eq. (4):

$$R_L = \frac{1}{\left(1 + K_L C_o\right)} \tag{4}$$

where C_o (mg/L) is the highest initial concentration of 2,4-D. R_L values between 0 and 1 (Table 2) imply a favorable adsorption process [35].

3.3.1.2. Freundlich isotherm

The Freundlich isotherm model, on the other hand, suggests a heterogeneous surface with varying energies of

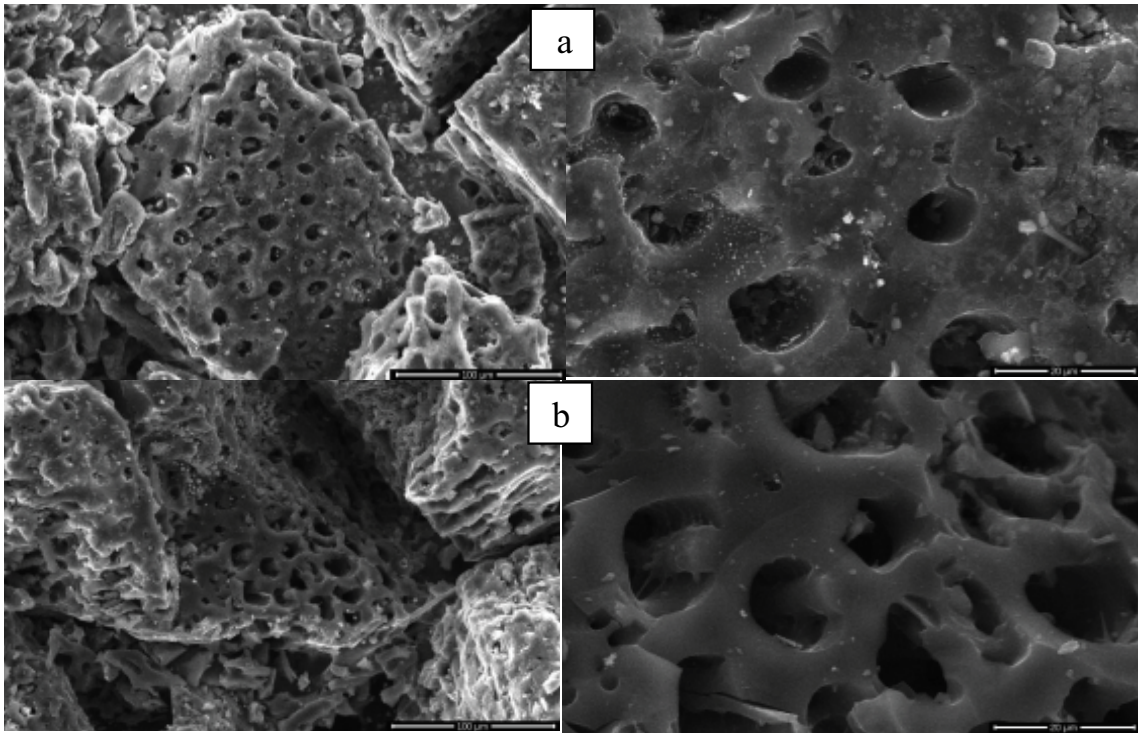

Fig. 4. Scanning electron microscopy image of BAC before adsorption (a), and after adsorption of 2,4-D (b).

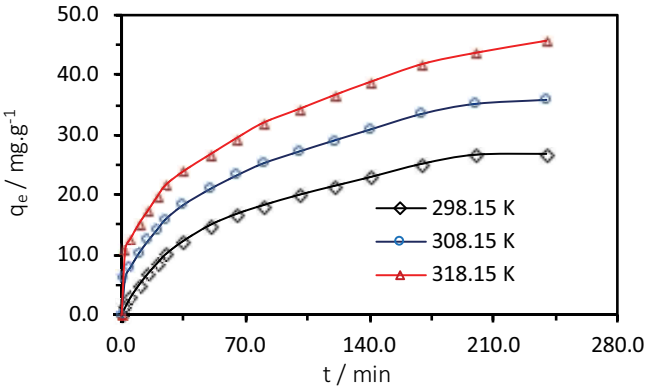

Fig. 5. Effect of contact time on the adsorption of 2,4-D onto BAC (2,4-D concentration = 80 mg/L, adsorbent dose = 0.80 g/L, and contact time = 240 min).

adsorption sites. It accounts for multilayer adsorption and allows for non-ideal behavior by introducing an empirical constant that represents the intensity of adsorption. This model can be expressed in the linear form by Hazzaa and Hussein [36] Eq. (5):

$$\ln q_e = \ln K_F + \frac{1}{n}\ln C_e \quad (5)$$

where K_F is the Freundlich isotherm constant and $1/n$ is the heterogeneity factor which can vary between 0 and 1, suggesting favorable adsorption process. The values of

Table 2
Isotherm parameters for the adsorption of 2,4-D onto BAC (two-parameter isotherms)

T (K)	298.15	308.15	318.15
Langmuir			
q_m	68.03	69.93	70.42
K_L	0.063	0.084	0.129
R_L	0.162	0.126	0.086
R^2	0.981	0.987	0.994
APE%	5.13	5.33	4.44
Freundlich			
$1/n$	0.621	0.585	0.518
K_F	5.69	7.47	10.79
R^2	0.936	0.928	0.929
APE%	12.22	13.12	12.40
Temkin			
B_T	14.87	15.21	15.25
A_T	0.65	0.88	1.33
R^2	0.997	0.999	0.996
APE%	2.11	1.36	2.45

K_F and n are calculated from the intercept and slope of the plot of $\ln q_e$ against $\ln C_e$ and listed in Table 3. Values of $1/n$ below one indicates normal adsorption, while values above $1/n$ imply cooperative adsorption.

3.3.1.3. Temkin isotherm

The Temkin isotherm model incorporates the effect of heat of sorption on the equilibrium constant. It assumes a linear decrease in heat of sorption with increasing coverage, due to adsorbate–adsorbate repulsions and uniformly distributed adsorption binding energies [37]. Additionally, this isotherm assumes that the decrease in heat of adsorption is linear, rather than logarithmic as implied in the Freundlich isotherm [38]. Temkin model is given by:

$$q_e = B_T \ln A_T + B_T \ln C_e \tag{6}$$

where B_T = (RT/b), it is related to the heat of adsorption (J/mol). T is the absolute temperature in K, R the universal gas constant, 8.314 J/mol·K, A_T the equilibrium binding constant (L/mg). By plotting q_e vs. lnC_e the constants A_T and B_T can be determined. The constants A_T and B_T are listed in Table 2.

The coefficient of determination (R^2) was used to test the best-fitting isotherm to the experimental data. R^2 is a statistical measure that shows how well the regression line fits the observed data points. It ranges from 0 to 1, with a value closer to 1 indicating a better fit.

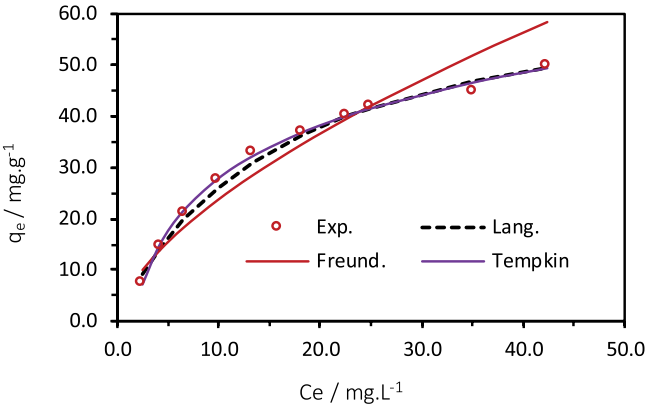

Fig. 6. Isothermal two parameter models for adsorption of 2,4-D on BAC (C_0 = (8–82) mg/L, BAC dosage = 0.80 g/L, equilibration time = 250 min, and temperature = 298.15 K).

$$R^2 = \frac{\sum_{i=1}^{N}\left(q_{e,\text{exp.}} - \overline{q_{e,\text{calc}}}\right)^2}{\sum_{i=1}^{N}\left(q_{e,\text{exp.}} - \overline{q_{e,\text{calc}}}\right)^2 + \sum_{i=1}^{N}\left(q_{e,\text{exp}} - q_{e,\text{calc}}\right)^2} \tag{7}$$

where $q_{e,\text{calc}}$ is the calculated equilibrium adsorbed amount, $q_{e,\text{exp}}$ is the measured equilibrium adsorbed amount and $\overline{q_{e,\text{calc}}}$ is the average of $q_{e,\text{calc}}$.

The average percentage error (APE%) is applied to minimize the fractional error distribution across the entire concentration range. Considering both positive and negative errors, the APE% offers a comprehensive analysis of the overall error in our measurements. By calculating the average percentage error, we can determine how much our measured values deviate from the true values on average. It is given by Eq. (8):

$$\text{APE\%} = \frac{\sum_{i=1}^{N}\left|\frac{q_{e,\text{exp.}} - q_{e,\text{pred.}}}{q_{e,\text{exp.}}}\right|}{N} \times 100 \tag{8}$$

where N is the number of experimental points.

Fig. 6 shows the experimental and the predicted data using two parameter isotherms for the adsorption of 2,4-D onto BAC at 298.15 K. It seems that the Temkin isotherm has the highest coefficient of determination and low average percentage error values when compared to Langmuir and Freundlich isotherms (Table 2).

Consequently, the Temkin isotherm can describe adequately the adsorption isotherms of 2,4-D onto BAC. Additionally, the heat of adsorption (B_T) in the Temkin model (Table 2) rests within the realm of physical adsorption at the investigated temperatures [39].

Table 3 compares the Langmuir adsorption capacities of 2,4-D by some other adsorbents reported in the literature with that of BAC.

3.3.2. Three-parameter models

3.3.2.1. Redlich–Peterson isotherm

The Redlich–Peterson isotherm, proposed by Redlich and Peterson [47], has been widely used to describe adsorption

Table 3
Comparison of 2,4-D Langmuir adsorption capacities of BAC with various activated carbons

Adsorbent	Adsorption capacity (mg/g)	Reference
Oil palm frond activated carbon	45.00 (at 30°C)	[40]
AC from cocoa pod husks	37.45 (at 30°C)	[41]
AC from pristine biomass	88.40	[42]
Chestnut shell AC	0.93 (at 35°C)	[43]
AC from filter paper and cotton	77.33	[44]
Algal magnetic activated carbon nanocomposite	60.61 (at 30°C)	[45]
AC from date palm coir waste	50.25	[46]
AC from *Balanites aegyptiaca* seed shell	68.03 (at 25°C)	This work
	69.93 (at 35°C)	
	70.42 (at 45°C)	

phenomena in various systems. One of the limitations of the Langmuir isotherm equation is its assumption of a homogeneous adsorbent surface, which may not hold true in many practical cases. On the other hand, the Freundlich isotherm equation considers heterogeneity but does not accurately describe certain adsorption systems due to its oversimplified assumptions.

The Redlich–Peterson isotherm offers a flexible method that can be employed in both heterogeneous and homogeneous systems by incorporating elements from both Langmuir and Freundlich equations. It has a linear and exponential dependence on equilibrium concentration in the numerator and the denominator, respectively. It can be described by Eq. (9):

$$q_e = \frac{k_R C_e}{1 + a_R C_e^{\beta}} \tag{9}$$

where k_R (L/g) and a_R (L/mg) are Redlich–Peterson isotherm constants, b is an exponent which lies between 0 and 1. At high concentrations of the adsorbate, Eq. (1) reduces to the Freundlich equation, where $k_R/a_R = K_F$ and $(1 - \beta) = 1/n$ of the Freundlich isotherm model. When b = 1, Eq. (5) reduces to Langmuir equation with $a_R = K_L$ (Langmuir adsorption constant (L/mg) and $k_R = K_L q_m$ where q_m is Langmuir maximum adsorption capacity of the adsorbent (mg/g). This isotherm model has versatile applications in either homogeneous or heterogeneous systems, displaying hybrid adsorption behavior.

3.3.2.2. Sips isotherm

Sips isotherm is a widely used model in adsorption studies, particularly for heterogeneous systems. It combines the characteristics of both Langmuir and Freundlich isotherms, making it a more versatile and accurate representation of adsorption behavior. The general expression for the Sips isotherm can be written by the study of Ayawei et al. [48]:

$$q_e = \frac{q_m \left(k_s C_e\right)^{n_s}}{1 + \left(k_s C_e\right)^{n_s}} \tag{10}$$

where k_S (L/mg) is the Sips isotherm model constant and n_S is Sips isotherm exponent which describes the surface heterogeneity, limited from 0 to 1. At low adsorbate concentration this model effectively reduces to the Freundlich model, but at high adsorbate concentrations this model predicts a monolayer sorption capacity characteristic of the Langmuir isotherm.

3.3.2.3. Toth isotherm

The Toth isotherm model [49], suggested as an improvement to the Langmuir isotherm equation, presents a more precise representation for adsorption in heterogeneous systems with sub-monolayer coverage. While the Langmuir isotherm assumes a uniform surface and complete monolayer coverage, the Toth model considers the presence of multiple adsorption sites and incomplete surface coverage. The Toth isotherm model is given by Eq. (11):

$$q_e = \frac{q_{m,T} k_T C_e}{\left(1 + \left(k_T C_e\right)^t\right)^{1/t}} \tag{11}$$

where k_T is the Toth equilibrium constant, and (t) is the Toth model exponent that characterizes the heterogeneity of the adsorption system.

The three parameters of Eqs. (9)–(11) were obtained by maximizing the value of R^2 using a trial-and-error procedure using the solver adds-in with Microsoft's spreadsheet, Microsoft Excel. The parameters of these isotherms at three temperatures are given in Table 3 together with APE%.

Fig. 7 shows experimental data and the predicted equilibrium curves using non-linear method for the three parameter isotherms Redlich–Peterson, Sips and Toth. The correlation coefficient values were moderately good for all three-parameter models, and the average percentage of errors were comparable to each other (Table 4), which clearly implies that Redlich–Peterson, Sips, and Toth isotherms can fit the adsorption data of 2,4-D onto BAC.

The Redlich–Peterson exponent "b" value at different temperatures is close to unity (b = 0.970–0.976). This shows that the adsorption of 2,4-D onto BAC is compatible with the Langmuir model rather than the Freundlich model. The Toth isotherm exponent (t) is nearly unity (t = 0.925–0.956). It tells us that the adsorption process occurs on a homogenous surface [50].

3.4. Effect of pH on the adsorption

The amount of adsorbed 2,4-D for different solution pH values (2.0–12.0) is shown in Fig. 8. The equilibrium uptake of 2,4-D decreased from 145.5 to 81.8 mg/g with increasing pH from 2 to 12. At pH values lower than the pH_{pzc}, the carbon surface is positively charged. This positive charge can attract and bind with negatively charged species, leading to a higher adsorption capacity. As the pH increases above the pH_{pzc}, the carbon surface becomes less positively charged and may even become negatively charged.

This change in surface charge can affect the interaction between the absorbent (BAC) and adsorbate (2,4-D). In this

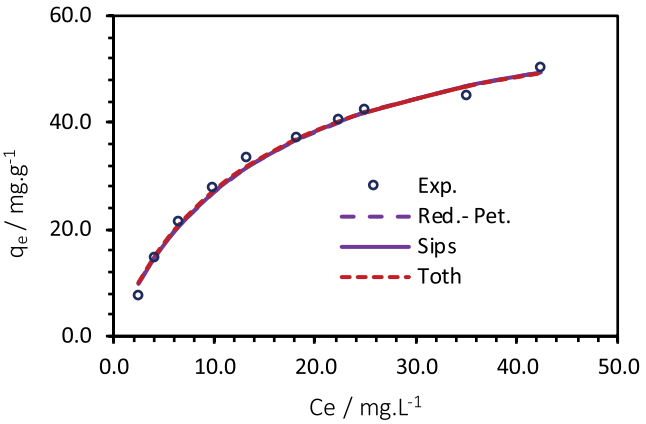

Fig. 7. Isothermal three parameter models for adsorption of 2,4-D on BAC. (C_0 = (8–82) mg/L, BAC dosage = 0.80 g/L, equilibration time = 250 min, and temperature = 298.15 K).

case, as the pH of the solution increased from 2 to 12, it moved further away from the pH_{pzc} value of 6.8. Consequently, the carbon surface became less positively charged and potentially more negatively charged. This change in surface charge likely reduced the attraction between BAC and 2,4-D molecules, resulting in a decrease in equilibrium uptake.

Additionally, changes in solution pH can also directly affect the chemical properties of 2,4-D itself. The acid dissociation constant (pK_a) of 2,4-D was 2.73 [51], hence the 2,4-D molecule was dissociated and existed in a large proportion of anions in solution when pH value was higher than pK_a. The degree of dissociation increased with increasing pH value and therefore decreasing the electrostatic attraction between more deprotonated 2,4-D and negatively charged BAC surface. This result is consistent with that reported previously for the adsorption of 2,4-D onto activated carbons derived from different materials [52–54].

Table 4
Isotherm parameters for the adsorption of 2,4-D onto BAC (three-parameter isotherms)

T (K)	298.15	308.15	318.15
	Redlich–Peterson		
k_{RP}	4.782	6.609	9.922
a_{RP}	0.080	0.109	0.160
b	0.976	0.972	0.970
R^2	0.993	0.994	0.994
APE%	5.26	4.84	4.16
	Sips		
q_m	67.110	68.510	73.209
k_s	0.067	0.091	0.118
n_s	0.983	0.987	0.938
R^2	0.993	0.994	0.992
APE%	5.17	4.88	4.74
	Toth		
q_{mT}	66.882	70.780	71.056
k_T	0.073	0.094	0.146
t	0.956	0.931	0.925
R^2	0.993	0.994	0.993
APE%	5.34	4.95	4.07

3.5. Effect of temperature on 2,4-D adsorption

Thermodynamics describes the energy changes that occur during an adsorption process. The thermodynamic parameters can provide insights into the mechanism of adsorption and the feasibility of the process.

The effect of temperature on 2,4-D adsorption onto BAC was studied by performing experiments at 25°C, 35°C and 45°C. Results showed that 2,4-D adsorption capacity increased with increasing temperature, (Fig. 9) showing that the adsorption was endothermic. temperature affects both the adsorption capacity in equilibrium experiments and the adsorption rates in batch kinetic experiments. The increase in adsorption ability of BAC at higher temperatures may be attributed to the enlargement of pore size, activation of the adsorbent surface, or creation of new pores on the adsorbent surface due to bond rupture. Additionally, it may be due to the heightened mobility of 2,4-D molecules from the bulk solution towards the adsorbent surface and the extent of penetration within the BAC structure, enhancing the rate of intraparticle diffusion.

To calculate the enthalpy change ($\Delta H°$), entropy change ($\Delta S°$) and free energy change ($\Delta G°$) for the investigated adsorption process, $\Delta H°$, $\Delta S°$ and $\Delta G°$ the Eqs. (12)–(15) [55]:

$$k_d = \frac{C_o - C_e}{C_e} \tag{12}$$

$$\Delta G° = -RT \ln k_d \tag{13}$$

$$\Delta G° = \Delta H° - T\Delta S° \tag{14}$$

From Eq. (13) and Eq. (14):

$$\ln k_d = \frac{\Delta S°}{R} - \frac{\Delta H°}{RT} \tag{15}$$

where k_d is the distribution coefficient (mL/g). The values of $\Delta H°$ and $\Delta S°$ are calculated from the slope and intercepts

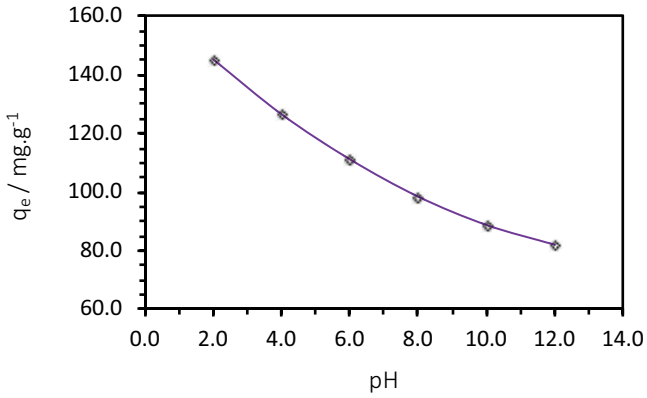

Fig. 8. Effect of pH on the adsorption of 2,4-D onto BAC at 298.15 K.

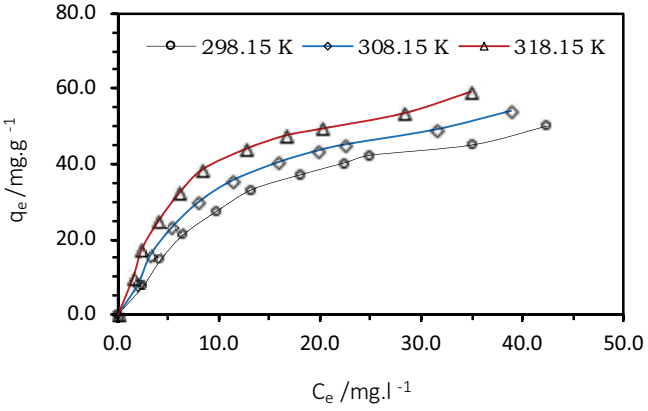

Fig. 9. Effect of temperature on the adsorption of 2,4-D onto BAC.

of the linear plot of $\ln k_d$ vs. $1/T$ (Table 5). Once these two parameters are obtained, $\Delta G°$ is calculated using the Eq. (14).

Negative values of $\Delta G°$ at different temperatures indicate the spontaneous sorption process of 2,4-D onto BAC. The positive values of $\Delta H°$ confirm the endothermic nature of adsorption. Positive values of entropy change show an increase in the randomness of the system before and after adsorption. These results agree with the observations made by Goscianska and Olejnik [56] for the removal of 2,4-D herbicide from an aqueous solution by aminosilane-grafted mesoporous carbons, and those concluded by Aksu and Kabasakal [57] for the adsorption of 2,4-D from an aqueous solution by granular activated carbon.

3.6. Adsorption kinetics

Kinetic models describe the rate at which adsorption occurs and the time needed to reach equilibrium. They are crucial in understanding the efficiency of adsorbent materials for water treatment. The adsorption kinetics of 2,4-D onto BAC were investigated using the pseudo-first-order and pseudo-second-order models [8]. The pseudo-first-order kinetic equation is expressed as:

$$\ln\left(q_e - q_t\right) = \ln q_e - k_1 t \tag{16}$$

where q_t is the amount of 2,4-D herbicide adsorbed in time t (mg/g), t is the time (min), k_1 is the adsorption rate constant of pseudo-first-order model (min^{-1}). k_1 values were found from the slope of the linear plots of $\log(q_e - q_t)$ vs. t.

The pseudo-second-order model was defined by Eq. (17):

$$\frac{t}{q_t} = \frac{1}{k_2 q_e^2} + \frac{1}{q_e} t \tag{17}$$

where k_2 is the rate constant of pseudo-second-order (g/mg·min). The term $k_2 q_e^2$ is the initial sorption rate, represented as $h = k_2 q_e^2$ (mg/g·min). The value of q_e and k_2 can be obtained by plotting t/q_t against t.

The kinetic data for the pseudo-first-order and pseudo-second-order models for the adsorption of 2,4-D in aqueous solution onto BAC were reported in Table 5. The R^2 values for the pseudo-second-order are close to unity at all temperatures studied, and therefore, this model is the most suitable for describing the adsorption of 2,4-D on BAC. Furthermore, the pseudo-second-order model calculation of q_e (mg/g) closely aligned with the experimental values, confirming suitability of the model. This result is in accord with many published reports for the removal of 2,4-D by activated carbon derived from biosorbents [58–60]. With increasing temperature, there was a corresponding increase in the values of both k_2 and h.

Table 5
Thermodynamic parameters for 2,4-D adsorption onto BAC at different temperatures

T (K)	$\Delta S°$ (J/mol·K)	$\Delta H°$ (kJ/mol)	$\Delta G°$ (kJ/mol)
298.15			–1.472
308.15	85.97	24.16	–2.332
318.15			–3.191

3.7. Adsorption mechanism

The intraparticle diffusion model is proposed to analyze the mechanism of the adsorption. The model is used fundamentally to prognosticate whether the intraparticle diffusion of particles is a rate-determining step or not. The intraparticle diffusion model is expressed by Eq. (18) [61]:

$$q_t = k_i t^{0.5} + C \tag{18}$$

where k_i is the intraparticle diffusion rate constant (mg/g·$min^{1/2}$), C (mg/g) gives an idea about the boundary layer thickness, that is, the larger the intercept, the greater is the boundary layer effect.

The intraparticle diffusion plot for the adsorption of 2,4-D onto BAC is shown in Fig. 10. The existence of two linear segments have been noticed to explain the two consecutive adsorption phases: initial mass transfer at a maximum limit of 50 min (steep portion) then followed by intraparticle diffusion of 2,4-D onto BAC (gradual portion). The observation of these two intercepting lines is a typical outcome when the adsorption phases operate independently, depending upon the exact mechanism.

The values of the pore diffusion parameters k_{i_1} and k_{i_2} for the two stages were calculated from the plots of linear portions of the curves (Table 6). The presence of the two diffusion stages shows that the pores of BAC have two perceptible sizes (macropores and mesopores). Values of k_{i_1} and k_{i_2} increase with increasing temperature which shows the enhanced diffusion of 2,4-D through the meso- and micropores at higher temperatures. Differences seen during straight lines departing from the origin (as depicted in Fig. 10) might result from a discrepancy between rates of adsorption during early and late stages [62]. Furthermore, the deviation in the slope value from 0.5 shows that diffusion through the pores is one of the rate-controlling steps [63].

Additionally, the kinetic data were analyzed using the Boyd model [64] to predict the rate-controlling step in the adsorption process. The Boyd model could be expressed as:

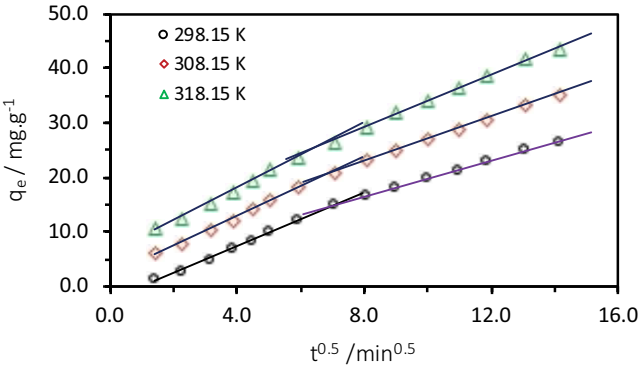

Fig. 10. Intraparticle diffusion plot for the adsorption of 2,4-D onto BAC. (2,4-D concentration = 80 mg/L, adsorbent dose = 1 g/L, contact time = 240 min).

Table 6
Kinetic parameters for 2,4-D adsorption by BAC

T (K)	Pseudo-first-order model				Pseudo-second-order model				
	$q_{e(exp)}$	$q_{e(calc)}$	k_1	R^2	$q_{e(exp)}$	$q_{e(calc)}$	k_2	h	R^2
298.15	26.80	25.60	1.51 E-02	0.998	26.80	32.89	5.42E-04	0.586	0.999
308.15	34.54	29.37	1.32 E-02	0.992	34.54	38.76	7.67E-04	1.152	0.995
318.15	43.04	33.94	1.16 E-02	0.985	43.04	45.94	9.13E-04	1.927	0.990

T (K)	Intraparticle diffusion model					
	k_{i_1}	C_1	R_1^2	k_{i_2}	C_2	R_2^2
298.15	2.507	–	0.997	1.393	6.285	0.963
308.15	2.814	1.766	0.996	1.532	12.140	0.967
318.15	3.202	5.870	0.996	1.819	16.365	0.971

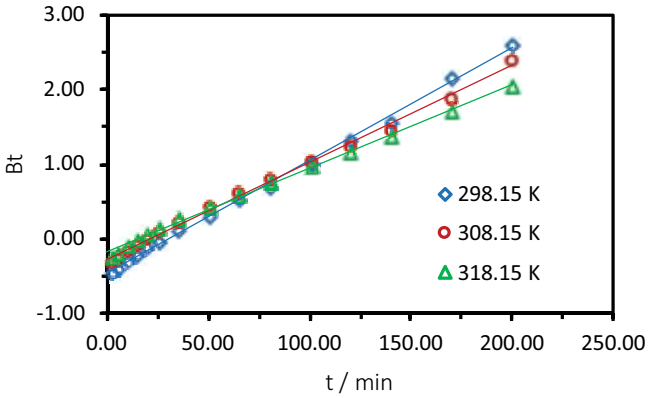

Fig. 11. Boyd plots for 2,4-D adsorption on BAC. (2,4-D concentration = 80 mg/L, adsorbent dose = 1 g/L, contact time = 240 min).

$$B_t = -0.4977 - \ln\left(1 - \frac{q_t}{q_e}\right) \tag{19}$$

Fig. 11 illustrates the Boyd plots for the adsorption of 2,4-D on BAC at different temperatures. The plots are close to being linear ($0.996 \le R^2 \le 0.998$), and the regression curves approach the origin, which implies that the adsorption of 2,4-D on BAC is controlled by the pore diffusion mechanism.

4. Conclusion

In this work, we explored the adsorption of 2,4-D onto low-cost activated carbon prepared from *Balanites aegyptiaca* seed shells (BAC). The presence of oxygen-containing functional groups on the surface of BAC was accurately identified through the FTIR technique and Boehm titration method. BAC had a relatively large surface area (417.0 m^2/g).

The Langmuir, Freundlich, and Temkin adsorption models were used to fit the adsorption equilibrium data of 2,4-D by BAC. The Temkin adsorption isotherm closely matched the experimental data within the tested concentrations. The three-parameter adsorption isotherm models (Redlich–Peterson, Sips, and Toth) were the models that best fit the adsorption data over the concentration range used and at all temperatures studied.

2,4-D adsorption capacity was increased with increasing temperature, while the removal efficiency of 2,4-D decreased with increasing solution pH. The thermodynamic study showed that adsorption was endothermic with positive values of $\Delta H°$ (24.16 kJ/mol) and $\Delta S°$ (85.97 J/mol·K). Meanwhile, negative values of $\Delta G°$ for the process of adsorption of 2,4-D at all analyzed temperatures indicate that the process is spontaneous.

The uptake pattern of 2,4-D was found to be primarily influenced by a pore diffusion process. The kinetic data obtained from the experiment was found to be in excellent agreement with a pseudo second-order model. The adsorption data obtained from this research study provides valuable insights into the potential of using BAC as a low-cost adsorbent for the removal of 2,4-D herbicide from aqueous solutions. Furthermore, the efficient removal of 2,4-D herbicide by BAC suggests its potential application in water treatment systems.

References

[1] K. Kusmierek, M. Sankowska, A. Swiatkowski, Kinetic and equilibrium studies of simultaneous adsorption of monochlorophenols and chlorophenoxy herbicides on activated carbon, Desal. Water Treat., 52 (2014) 178–183.
[2] A.M. Youssef, H. El-Didamony, S.F. El-Sharabasy, M. Sobhy, A.F. Hassan, R. Bolaneke, Adsorption of 2,4-dichlorophenoxyacetic acid on different types of activated carbons-based date palm pits: kinetic and thermodynamics studies, Int. Res. J. Pure Appl. Chem., 14 (2017) 1–15.
[3] H. Zhang, X. Yuan, T. Xiong, H. Wang, L. Jiang, Bioremediation of co-contaminated soil with heavy metals and pesticides: influence factors, mechanisms and evaluation methods, Chem. Eng. J., 398 (2020) 125657, doi: 10.1016/j.cej.2020.125657.
[4] Z. Aksu, E. Kabasakal, Adsorption characteristics of 2,4-dichlorophenoxyacetic acid (2,4-D) from aqueous solution on powdered activated carbon, J. Environ. Sci. Health., Part B, 40 (2005) 545–570.
[5] R.M. Madero-Castro, J.M. Vicent-Luna, X. Peng, S. Calero, Adsorption of linear alcohols in amorphous activated carbons: implications for energy storage applications, ACS Sustainable Chem. Eng., 10 (2022) 6509−6520.
[6] M.M. Bade, A.A. Dubale, D.F. Bebizuh, M. Atlabachew, Highly efficient multisubstrate agricultural waste-derived activated carbon for enhanced CO_2 capture, ACS Omega, 7 (2022) 18770−18779.
[7] A.I. Abd-Elhamid, M. Emran, M.H. El-Sadek, A.A. El-Shanshory, H.M.A. Soliman, A.M. Awwad, M. Rashad, Enhanced removal

of cationic dye by eco-friendly activated biochar derived from rice straw, Appl. Water Sci., 10 (2020) 45, doi: 10.1007/s13201-019-1128-0.
[8] S. Usanmaz, Ç. Özer, M. İmamoğlu, Removal of Cu(II), Ni(II) and Co(II) ions from aqueous solutions by hazelnut husks carbon activated with phosphoric acid, Desal. Water Treat., 227 (2021) 300–308.
[9] S. Tünay, R. Köklü, M. İmamoğlu, Removal of diclofenac, ciprofloxacin and sulfamethoxazole from wastewater using granular activated carbon from hazelnut shell: isotherm, kinetic and thermodynamic studies, Desal. Water Treat., 277 (2022) 155–168.
[10] A.T. Adeolu, O.T. Okareh, A.O. Dada, Adsorption of chromium ion from industrial effluent using activated carbon derived from plantain (*Musa paradisiaca*) wastes, Am. J. Environ. Prot., 4 (2016) 7–20.
[11] H.O. Chukwuemeka-Okorie, F.K. Ekuma, K.G. Akpomie, J.C. Nnaji, A.G. Okereafor, Adsorption of tartrazine and sunset yellow anionic dyes onto activated carbon derived from cassava sievate biomass, Appl. Water Sci., 11 (2021) 27, doi: 10.1007/s13201-021-01357-w.
[12] H.Y. Wu, S.S. Chen, W. Liao, W. Wang, M.F. Jang, W.H. Chen, T. Ahamad, S.M. Alshehri, C.H. Hou, K.S. Lin, T. Charinpanitkul, K.C. Wu, Assessment of agricultural waste-derived activated carbon in multiple applications, Environ. Res., 191 (2020) 110176, doi: 10.1016/j.envres.2020.110176.
[13] U. Yunusa, B. Usman, M. Ibrahim, Modeling and regeneration studies for the removal of crystal violet using *Balanites aegyptiaca* seed shell activated carbon, J. Turk. Chem. Soc. Sect. A Chem., 8 (2021) 195–208.
[14] Y. Umar, I.K. Abdulrahman, A. Yusuf, A. Tahir, H. Musa, Hexavalent chromium removal from simulated wastewater using biomass-based activated carbon: kinetics, mechanism, thermodynamics and regeneration studies, Alger. J. Eng. Technol., 4 (2021) 29–44.
[15] G. Wyasu, H.T. Rumah, S. Moses, Batch adsorption of Hg^{2+} and As^{3+} ions in hospital wastewater using activated carbon from *Balanites aegyptiaca* and Detarium microcarpum, Commun. Phys. Sci., 5 (2020) 611–618.
[16] E.E. Mon, T. Hirata, K. Kawamoto, S. Hiradate, T. Komatsu, P. Moldrup, Adsorption of 2,4-dichlorophenoxyacetic acid onto volcanic ash soils: effects of pH and soil organic matter, Environ. Asia, 1 (2009) 1–9, doi: 10.14456/ea.2009.1.
[17] M. Pirsaheb, A. Dargahi, S. Hazrati, M. Fazlzadehdavil, Removal of diazinon and 2,4-dichlorophenoxy-acetic acid (2,4-D) from aqueous solutions by granular activated carbon, Desal. Water Treat., 52 (2014) 4350–4355.
[18] Guidelines for Drinking-Water Quality, Fourth Edition Incorporating the First Addendum, World Health Organization, Geneva, 2017, pp. 347–348.
[19] H. Zhang, J. Wang, Y. Teng, S. Jia, H. Huang, Y. Li, C. Wang, Ce-MOF composite electrospinning as antibacterial adsorbent for the removal of 2,4-dichlorophenoxyacetic acid, Chem. Eng. J., 462 (2023) 142195, doi: 10.1016/j.cej.2023.142195.
[20] H.N. Tran, H.-P. Chao, S.-J. You, Activated carbons from golden shower upon different chemical activation methods: synthesis and characterizations, Adsorpt. Sci. Technol., 36 (2018) 95–113.
[21] R. Abubeah, H. Altaher, T.E. Khalil, Removal of hexavalent chromium using two innovative adsorbents, Environ. Eng. Manage. J., 17 (2018) 1621–1634.
[22] T. Skripkina, E. Podgorbunskikh, A. Bychkov, O. Lomovsky, Sorption of methylene blue for studying the specific surface properties of biomass carbohydrates, Coatings, 10 (2020) 1115, doi: 10.3390/coatings10111115.
[23] B.T. Brij, O.T. Clint, Use of basic methylene blue dye for specific surface area measurement of metal hexacyanoferrate(II) complexes, Rev. Soc. Quím. Perú, 74 (2010) 330–335.
[24] A.U. Itodo, H.U. Itodo, M.K. Gafar, Estimation of specific surface area using Langmuir isotherm method, J. Appl. Sci. Environ. Manage., 14 (2010) 141–145.
[25] D.L. Pavia, G.M. Lampman, G.S. Kriz, J.R. Vyvyan, Introduction to Spectroscopy, 4th ed., Brooks Cole Cengage Learning, USA, 2008, pp. 46–48.
[26] N.S. Trivedi, R.A. Kharkar, S.A. Mandavgane, 2,4-dichlorophenoxyacetic acid adsorption on adsorbent prepared from groundnut shell: effect of preparation conditions on equilibrium adsorption capacity, Arabian J. Chem., 12 (2019) 4541–4549.
[27] Y.F. Jia, K.M. Thomas, Adsorption of cadmium ions on oxygen surface sites in activated carbon, Langmuir, 16 (2006) 1114–1122.
[28] Z. Belala, M. Jeguirim, M. Belhachemi, F. Addoun, G. Trouvé, Biosorption of basic dye from aqueous solutions by date stones and palm-trees waste: kinetic, equilibrium and thermodynamic studies, Desalination, 271 (2011) 80–87.
[29] C. Bouchelta, M.S. Medjram, O. Bertrand, J.P. Bellat, Preparation and characterization of activated carbon from date stones by physical activation with steam, J. Anal. Appl. Pyrolysis, 82 (2008) 70–77.
[30] N. El Messaoudi, M. El Khomri, S. Bentahar, A. Dbik, A. Lacherai, B. Bakiz, Evaluation of performance of chemically treated date stones: application for the removal of cationic dyes from aqueous solutions, J. Taiwan Inst. Chem. Eng., 67 (2016) 244–253.
[31] B. Virote, S. Srisuda, T. Wiwut, Preparation of activated carbons from coffee residue for the adsorption of formaldehyde, Sep. Purif. Technol., 42 (2005) 159–168.
32] A.A. El-Hendawy, Variation in the FTIR spectra of a biomass under impregnation, carbonization and oxidation conditions, J. Anal. Appl. Pyrolysis, 75 (2006) 159–166.
[33] S.A. Kalam, M.S. Abu-Khamsin, Kamal, S. Patil, Surfactant adsorption isotherms: a review, ACS Omega, 6 (2021) 32342–32348.
[34] D. Xiao, W. Ding, J. Zhang, Y. Ge, Z. Wu, Z. Li, Fabrication of a versatile lignin-based nano-trap for heavy metal ion capture and bacterial inhibition, Chem. Eng. J., 358 (2019) 310–320.
[35] M.S.I. Syafiqah, H.W. Yussof, Kinetics, isotherms, and thermodynamic studies on the adsorption of mercury(II) ion from aqueous solution using modified palm oil fuel ash, Mater. Today Proc., 5 (2018) 21690–21697.
[36] R. Hazzaa, M. Hussein, Adsorption of cationic dye from aqueous solution onto activated carbon prepared from olive stones, Environ. Technol. Innovation, 4 (2015) 36–51.
[37] D. Kavitha, C. Namasivayam, Experimental and kinetic studies on methylene blue adsorption by coir pith carbon, Bioresour. Technol., 98 (2007) 14–21.
[38] T. Kameda, K. Horikoshi, S. Kumagai, Y. Saito, T. Yoshioka, Adsorption of urea, creatinine, and uric acid onto spherical activated carbon, Sep. Purif. Technol., 237 (2020) 116367, doi: 10.1016/j.seppur.2019.116367.
[39] B. Zhang, S. Yu, Y. Zhu, Y. Shen, X. Gao, W. Shi, J.-H. Tay, Adsorption mechanisms of crude oil onto polytetrafluoroethylene membrane: kinetics and isotherm, and strategies for adsorption fouling control, Sep. Purif. Technol., 235 (2020) 116212, doi: 10.1016/j.seppur.2019.116212.
[40] J.M. Salman, V.O. Njoku, B.H. Hameed, Batch and fixed-bed adsorption of 2,4-dichlorophenoxyacetic acid onto oil palm frond activated carbon, Chem. Eng. J., 174 (2011) 33–40.
[41] O.V. Anumasahun, A.O. Akinola, O.O. Bello, O.S. Agboola, O.S. Bello, Removal of 2,4-dichlorophenol from aqueous medium using activated carbon prepared from cocoa pod husks, Chem. Data Collect., 44 (2023) 100997, doi: 10.1016/j.cdc.2023.100997.
[42] S. Deng, R. Ma, Q. Yu, J. Huang, G. Yu, Enhanced removal of pentachlorophenol and 2,4-D from aqueous solution by an aminated biosorbent, J. Hazard. Mater., 165 (2009) 408–414.
[43] J. Gülen, S. Aslan, Adsorption of 2,4-dichlorophenoxyacetic acid from aqueous solution using carbonized chestnut as low cost adsorbent: kinetic and thermodynamic, Z. Phys. Chem., 234 (2020) 461–484.
[44] M. Khoshnood, S. Azizian, Adsorption of 2,4-dichlorophenoxyacetic acid pesticide by graphitic carbon nanostructures prepared from biomasses, J. Ind. Eng. Chem., 18 (2012) 1796–1800.
[45] R. Vinayagam, S. Ganga, G. Murugesan, G. Rangasamy, R. Bhole, L.C. Goveas, T. Varadavenkatesan, N. Dave, A. Samanth, V.R. Devi, R. Selvaraj, 2,4-Dichlorophenoxyacetic

acid (2,4-D) adsorptive removal by algal magnetic activated carbon nanocomposite, Chemosphere, 310 (2023) 136883, doi: 10.1016/j.chemosphere.2022.136883.
[46] K. Rambabu, J. AlYammahi, G. Bharath, A. Thanigaivelan, N. Sivarajasekar, F. Banat, Nano-activated carbon derived from date palm coir waste for efficient sequestration of noxious 2,4-dichlorophenoxyacetic acid herbicide, Chemosphere, 282 (2021) 131103, doi: 10.1016/j.chemosphere.2021.131103.
[47] O. Redlich, D.L. Peterson, A useful adsorption isotherm, J. Phys. Chem., 63 (1959) 1024, doi: 10.1021/j150576a611.
[48] N. Ayawei, A.N. Ebelegi, D. Wankasi, Modelling and interpretation of adsorption isotherms, J. Chem., 2017 (2017) 3039817, doi: 10.1155/2017/3039817.
[49] J. Toth, Calculation of the BET-compatible surface area from any Type I isotherms measured above the critical temperature, J. Colloid Interface Sci., 225 (2000) 378–383.
[50] M. Brdar, M. Šćiban, A. Takači, T. Došenović, Comparison of two and three parameters adsorption isotherm for Cr(VI) onto Kraft lignin, Chem. Eng. J., 183 (2012) 108–111.
[51] Q. Li, J. Sun, T. Ren, L. Guo, Z. Yang, Q. Yang, H. Chen, Adsorption mechanism of 2,4-dichlorophenoxyacetic acid onto nitric-acid-modified activated carbon fiber, Environ. Technol., 39 (2018) 895–906.
[52] J. Salman, B. Hameed, Adsorption of 2,4-dichlorophenoxyacetic acid and carbofuran pesticides onto granular activated carbon, Desalination, 256 (2010) 129–135.
[53] G. Wu, X. Sun, H. Hui, X. Zhang, J. Yan, Q. Zhang, Adsorption of 2,4-dichlorophenol from aqueous solution by activated carbon derived from moso bamboo processing waste, Desal. Water Treat., 51 (2013) 4603–4612.
[54] H.M.N. Hazrin, A. Lim, C. Li, J.J. Chew, J. Sunarso, Adsorption of 2,4-dichlorophenoxyacetic acid onto oil palm trunk-derived activated carbon: isotherm and kinetic studies at acidic, ambient condition, Mater. Today Proc., 64 (2022) 1557–1562.
[55] A.A. Nayla, I.M. Ahmed, A.I. Abd-Elhamid, H.F. Aly, M.F. Attallah, Selective sorption of ^{134}Cs and ^{60}Co radioisotopes using synthetic nano-copper ferrocyanide-SiO_2 materials, Sep. Purif. Technol., 234 (2020) 116060, doi: 10.1016/j.seppur.2019.116060.
[56] J. Goscianska, A. Olejnik, Removal of 2,4-D herbicide from aqueous solution by aminosilane-grafted mesoporous carbons, Adsorption, 25 (2019) 345–355.
[57] Z. Aksu, E. Kabasakal, Batch adsorption of 2,4-dichlorophenoxy-acetic acid (2,4-D) from aqueous solution by granular activated carbon, Sep. Purif. Technol., 35 (2004) 223–240.
[58] V. Njoku, B. Hameed, Preparation and characterization of activated carbon from corncob by chemical activation with H_3PO_4 for 2,4-dichlorophenoxyacetic acid adsorption, Chem. Eng. J., 173 (2011) 391–399.
[59] M. Dehghani, S. Nasseri, M. Karamimanesh, Removal of 2,4-dichlorophenolyxacetic acid (2,4-D) herbicide in the aqueous phase using modified granular activated carbon, J. Environ. Health Sci. Eng., 12 (2014) 28, doi: 10.1186/2052-336X-12-28.
[60] A. Samanth, R. Vinayagam, G. Murugesan, T. Varadavenkatesan, R. Selvaraj, A. Pugazhendhi, Enhanced adsorption of 2,4-dichlorophenoxyacetic acid using low-temperature carbonized *Peltophorum pterocarpum* pods and its statistical physics modeling, Chemosphere, 336 (2023) 139143, doi: 10.1016/j.chemosphere.2023.139143.
[61] A.M. Awad, R. Jalab, A. Benamor, M.S. Nasser, M.M. Ba-Abbad, M. El-Naas, A. Mohammad, Adsorption of organic pollutants by nanomaterial-based adsorbents: an overview, J. Mol. Liq., 301 (2020) 112335, doi: 10.1016/j.molliq.2019.112335.
[62] A.K. Sahu, V.C. Srivastava, I.D. Mall, D.H. Lataye, Adsorption of furfural from aqueous solution onto activated carbon: kinetic, equilibrium and thermodynamic study, Sep. Sci. Technol., 43 (2008) 1239–1259.
[63] N. Kannan, M.M. Sundaram, Kinetics and mechanism of removal of methylene blue by adsorption on various carbons-a comparative study, Dyes Pigm., 51(2001) 25–40.
[64] J. Wang, X. Guo, Adsorption kinetic models: physical meanings, applications, and solving methods, J. Hazard. Mater., 390 (2020) 122156, doi: 10.1016/j.jhazmat.2020.122156.